Design of a Transonic Wing with an Adaptive Morphing Trailing Edge via Aerostructural Optimization

David A. Burdette[a], Joaquim R. R. A. Martins[a,*]

[a] *University of Michigan, Department of Aerospace Engineering*

Abstract

Novel aircraft configurations and technologies like adaptive morphing trailing edges offer the potential to improve the fuel efficiency of commercial transport aircraft. To accurately quantify the benefits of morphing wing technology for commercial transport aircraft, high-fidelity design optimization that considers both aerodynamic and structural design with a large number of design variables is required. To address this need, we use high-fidelity aerostructural that enables the detailed optimization of wing shape and sizing using hundreds of design variables. We perform a number of multipoint aerostructural optimizations to demonstrate the performance benefits offered by morphing technology and identify how those benefits are enabled. In a comparison of optimizations considering seven flight conditions, the addition of a morphing trailing edge device along the aft 40% of the wing can reduce cruise fuel burn by more than 5%. A large portion of fuel burn reduction due to morphing trailing edges results from a significant reduction in structural weight, enabled by adaptive maneuver load alleviation. We also show that a smaller morphing device along the aft 30% of the wing produces nearly as much fuel burn reduction as the larger morphing device, and that morphing technology is particularly effective for high aspect ratio wings.

Keywords: Morphing, Adaptive compliant trailing edge, Wing design, Aerostructural optimization, Common Research Model

*Corresponding author

1. Introduction

Increased awareness of environmental concerns and fluctuations in fuel prices in recent years have led the aircraft manufacturing industry to push for improved aircraft fuel efficiency. Compared to the rapid improvements in aircraft fuel efficiency seen between 1960 and 1990, the rate of improvement in recent decades has been more moderate. Decades of experience and design refinement have left only relatively small improvements to be made on conventional wing and tube configurations. The combination of increased interest in reducing fuel burn and the recent plateau of fuel burn improvements with a conventional configuration has pushed aircraft manufacturers and researchers to consider new technologies and configurations that offer the potential for further efficiency improvements. In the long term, new unconventional aircraft configurations offer promising potential; however, they are likely a few decades from commercial availability. There are also a number of technologies that are closer to entering the market and offer efficiency improvements on conventional configurations, like tow-steered composites [1] and functionally graded materials [2].

Another such technology is adaptable morphing trailing edge, also known as adaptive compliant trailing edge, or simply adaptive trailing edge [3]. Companies such as FlexSys have already developed such devices [4, 5, 6] and have performed flight tests in collaboration with NASA and the U.S. Air Force Research Laboratory [7]. This technology offers the potential to create wings that can actively adapt to flight conditions, enabling engineers to design the wing shape and sizing with much more robust performance with respect to the flight conditions. Another variant of this technology is the variable camber continuous trailing edge flap, which changes the camber using three segments that rotate rigidly [8, 9].

Various studies have reviewed morphing mechanisms [10, 11, 12, 13] and explored and reviewed the benefits of applying this technology to wing design [14, 15, 16, 17, 18]. In the late nineties, Hanselka [19] and Monner *et al.* [20] outlined the aerodynamic benefits associated with morphing trailing edge de-

vices and offered designs for morphing mechanisms. More recently, Molinari *et al.* [21, 22] explored the potential of the technology using a multidisciplinary optimization approach considering mission, aerodynamic, materials, and structural disciplines. That work used low fidelity models and therefore was unable to capture the effects of small shape changes, which have been shown to be crucial in transonic aerodynamic performance [23]. Reynolds-averaged Navier–Stokes (RANS) simulations are required to capture the viscous and compressibility effects in that flight regime. Lyu and Martins [24] used RANS-based aerodynamic shape optimizations to design a wing with a morphing trailing edge showing drag reductions between one and five percent, depending on the flight condition. Wakayama *et al.* [25] found similar results in their work considering morphing devices on three different aircraft configurations. Other studies have also considered dynamic aeroelastic constraints [26]. Multidisciplinary design optimization (MDO) provides the computational approach to make the most of these technologies [27].

We have previously used MDO coupling high-fidelity models of the aerodynamics and structures to evaluate a wing with a morphing trailing edge at a single cruise point [28], showing that the morphing trailing edge can drastically affect the wing spanwise lift distribution. In the work presented herein, we seek to build off of these previous results by expanding the number of flight conditions where the performance of the wing is considered. The main advantage of morphing trailing edge technology is its ability to adapt a wing to changing flight conditions, so we expect multipoint analysis to provide better opportunities for the morphing trailing edge to improve performance. The inclusion of structural analysis is also important, as structural deflections will vary at different flight conditions, providing further opportunity for the morphing trailing edge to improve performance. In this work, we assume an ideal morphing mechanism that can achieve the specified shape, where the weight of the mechanism is comparable to that of conventional control actuators. While this is not a realistic assumption, these studies provide an upper bound on the benefits of morphing technologies and open the door for more detailed studies using

high-fidelity aerostructural design optimization.

This paper is organized as follows: Section 2 describes the computational tools used in this work. Section 3 defines the optimization problems solved in this work, including baseline configurations, multipoint stencil definitions, and an overview of the optimization parameters. Section 4 presents the optimization results, followed by the conclusions in the last section.

2. Overview of numerical methods

In this section, we discuss the numerical analysis and design optimization algorithms used in this work. The numerical algorithms are implemented in components of the MACH (MDO for Aircraft Configurations with High fidelity) framework [29]. The tools outlined herein have been used on a wide variety of aerodynamic [23, 30, 31] and aerostructural aircraft design optimization problems [32, 33, 34] as well as optimizations of wind turbine blades [35] and hydrofoils [36].

2.1. Geometric parametrization

Geometric shape changes are parametrized using a Free Form Deformation (FFD) approach [37], a technique that is also used frequently in computer graphics to generate deformations of solid geometries [38]. The approach implants the solid geometry within an outer hull that is parametrized with a series of control points. The control points generate deformations of the encompassing volume, which are interpolated onto the geometry. The interpolation generates a region of influence spanning two control points in each (i, j, and k) parametric direction and provides smooth deformations that are defined with a relatively small number of design variables. Aggregating control points also allows for the creation of larger-scale global design variables such as chord, span, and twist. An example of an FFD used for a morphing trailing edge optimization is shown in Figure 1.

Note that the FFD does not have a uniform distribution of control points along the (chord-wise) x-direction. Instead, there is a grouping of control points

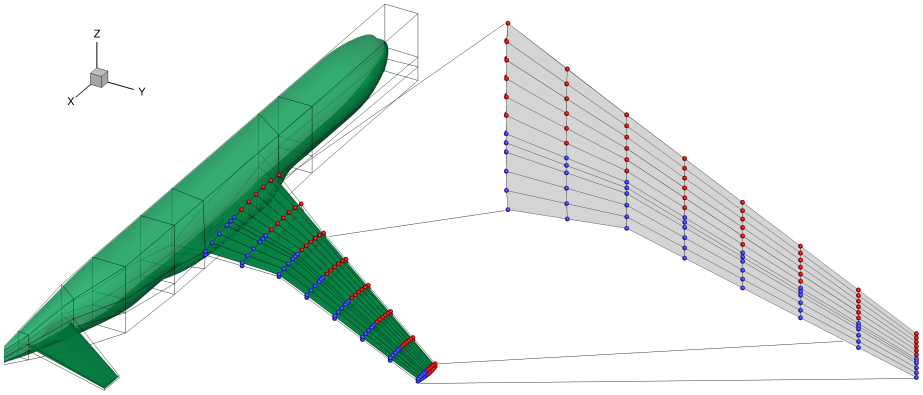

Figure 1: The control points in this shape parametrization are aligned with 30, 35, and 40% of the chord. Allowing the 4 aft-most rows of design variables to move results in a morphing device spanning the area enclosed by the blue control points.

near the leading edge of the morphing region. This control point distribution allows for simple implementation of the morphing trailing edge. The subset of the FFD control points on the aft region of the wing is given additional freedom at each flight condition, allowing the wing to assume different shapes at different flight conditions. The FFD is a tri-variate B-spline volume, so the geometric shape changes produced by a single control point moving are continuous changes restricted to a region spanning *exactly* two control points in each direction. Using this feature of the parameterization, we define the size of the morphing device using control point placement. The increased control point density near the boundary of the morphing region provides a parameterization that can generate smooth and rapid transitions between the morphing and fixed regions.

The use of FFD to parameterize morphing is not typical in the literature. Most morphing studies start with an assumed mechanism and simulate morphing using the restricted design space provided by that specific mechanism [21, 25, 26]. Examples of such morphing shape design spaces include a number of rigid rotations or a series of spanwise polynomial deformation profiles [9]. The morphing deformations produced using FFDs in this work represent a wider

design space. This less restrictive parameterization permits a wide variety of morphing shapes, which when coupled with gradient-based optimization allows the exploration of the potential of morphing technology, rather than the potential of a specific morphing mechanism. As such, the optimal morphing shapes presented in this paper are mechanism-independent optimal shapes. This approach is useful for quantifying the potential of general morphing technology, but it also informs the design of morphing mechanisms. Mechanisms capable of producing the morphing shapes found in the optimizations herein can provide the full benefit of morphing, while more restrictive mechanisms would yield reduced returns. The optimal shapes additionally demonstrate the types of deformations that are not needed for optimal returns. Mechanisms that enable these deformations are likely incurring an excessive weight penalty that should be removed (although a more complete analysis of all critical sizing conditions is required to definitively eliminate potential shapes). Given the diversity of morphing devices and their capabilities, we found optimization using this more general approach was preferable.

The FFD implementation used in this work also supports the creation and usage of nested FFDs, such as that used for the horizontal tail. A sub-FFD around the tail allows the optimizer to generate solid body rotation of the horizontal stabilizer, which is important for trimming the aircraft.

2.2. Mesh deformation

The nature of morphing trailing edge deformations makes mesh deformation a challenge, particularly during maneuver conditions where the mesh needs to deform according to both low frequency structural deformations and high frequency deformations from the morphing trailing edge. As such, we used an inverse-distance-weighting warping algorithm similar to that used by Luke *et al.* [39] in this work. The warping scheme interpolates both displacements and rotations of the surface into the volume mesh. One of the principal strengths of this approach is its ability to preserve mesh perpendicularity near surfaces. This feature is particularly valuable in the context of morphing trailing edge

optimizations, for which past experience has shown that other mesh warping schemes often generate negative cell volumes and mesh crossover near the deformed trailing edge. We used a KD-tree produced with an efficient spatial search algorithm to improve the computational performance of the warping.

2.3. CFD solver

The aerodynamic solver within the MACH framework is ADflow [40, 41], a finite-volume CFD solver for structured multiblock meshes. To provide sufficient fidelity for shape optimization of a transonic wing, ADflow solves the Reynolds-averaged Navier–Stokes (RANS) equations, with a one equation Spalart–Allmaras (SA) turbulence model. The flow is solved with a combination of Runge–Kutta (RK) and Newton–Krylov (NK) schemes. ADflow also computes gradients of the functions and constraints using a discrete adjoint approach, with partial derivatives computed with a combination of analytic and reverse mode automatic differentiation (AD) techniques [41]. With this implementation, the cost of computing a gradient is nearly independent of the number of design variables.

2.4. Structural solver

The structural solver in the MACH framework is the Toolkit for Analysis of Composite Structures (TACS) [42]. TACS is a parallel finite element solver designed for the analysis of aircraft structures, particularly the thin shell components typical of wing box members, which often lead to poorly conditioned matrices in the governing equations. Like ADflow, TACS also computes gradients using the adjoint method. Given the large number of elements where structural constraints need to be applied, TACS uses a Kreisselmeier–Steinhauser function aggregation to limit the number of functions of interest. This substantially reduces the number of required adjoint solves, and thus the overall computational cost of an optimization [43, 44].

2.5. Coupled aerostructural solver

The main role of the aerostructural solver is to couple the aerodynamic and structural solvers, ADflow and TACS. Structural deformations are transferred

to the aerodynamic mesh using a rigid link method [45, 46], in which the nodes of the aerodynamic mesh are associated with the nearest point of the structural model. The deformation of those points in the structure are then applied to their associated points in the aerodynamic mesh. To complete the coupling, a consistent force vector is constructed from the integrated aerodynamic forces and applied to the structure. The aerostructural solver solves the coupled nonlinear system of equations using a block Gauss–Seidel algorithm. As is the case with both of its components, the aerostructural solver also computes derivatives using the adjoint method [29].

2.6. Optimization algorithm

The optimizations in this work are performed using SNOPT (Sparse Nonlinear OPTimizer) [47], an optimization algorithm that uses a sequential quadratic programming (SQP) approach with a quasi-Newton approximation of the Hessian of the Lagrangian. This optimization method requires a relatively small number of function and gradient calculations, which is particularly important for aerostructural optimization where both function analyses and gradient computations are computationally expensive. We use SNOPT through pyOptSparse [48], a Python package that allows for the rapid formulation of nonlinear optimization problems and provides a common interface that facilitates benchmarking of different optimization algorithms [49].

3. Problem formulation

The initial configuration used in the optimizations is the undeflected Common Research Model (uCRM) [34]. The aerodynamic and structural meshes used for this configuration can be seen in Figure 2, superimposed with pressure and stress contours at the nominal flight condition. The top and bottom skins of the wingbox have been shifted to expose the ribs and rear spar. The aerodynamic model is a multiblock mesh with about 1.3 million cells. The structural model consists of 10,584 second-order mixed interpolation of tensorial components (MITC) shell elements.

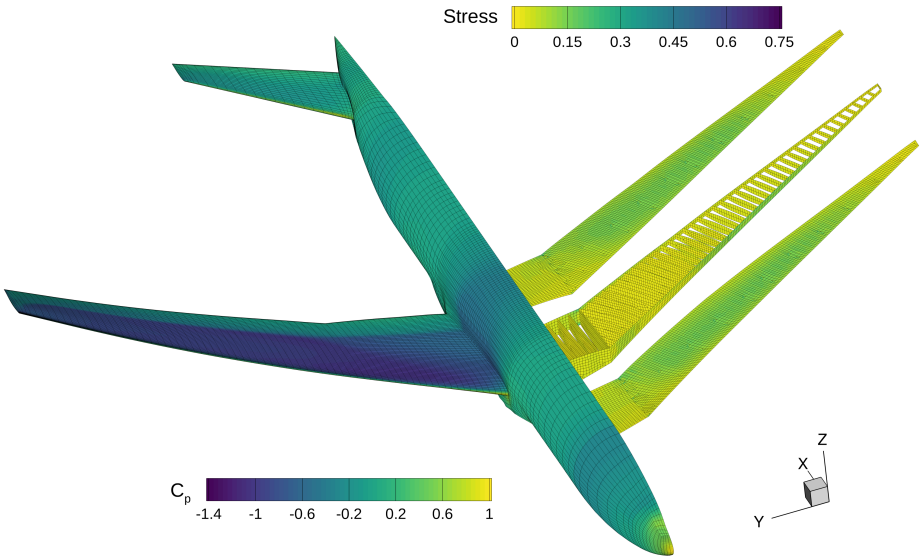

Figure 2: The baseline uCRM configuration with an aerodynamic (left) and a structural (right) solution at the nominal cruise condition superimposed with the corresponding computational meshes.

The wing is first optimized without any morphing capabilities to provide a fair reference from which to measure the improvements provided in subsequent morphing optimizations. Comparing the fuel burn of the optimized aircraft with and without the morphing design variables, we isolate and quantify the effects of the morphing trailing edge.

In the optimizations of the morphing wing, morphing design variables are included at all of the non-nominal flight conditions. The "baseline" or non-morphed wing shape is defined using design variables over the entire FFD at the nominal flight condition. Since that set of design variables defines the baseline shape of the wing, adding redundant variables in the morphing region is both unnecessary and inadvisable. Adding redundant morphing variables at the nominal cruise conditions produces an ill-posed optimization problem. Redundant design variables are, in general, unfavorable in optimization problems, as linear combinations of redundant variables can produce an infinite number of optimal solutions.

Flight condition	**Mach**	C_L	**Altitude (ft)**
Nominal	0.85	0.50	34,000
Low C_L	0.85	0.45	34,000
High C_L	0.85	0.55	34,000

Table 1: Overview of the 3-point stencil of cruise flight conditions. These three conditions are aligned vertically in Figure 3.

We consider two multipoint stencils: a 3-point stencil with varying lift coefficient and a 7-point stencil with varying lift coefficient, Mach number, and altitude. We have previously investigated the selection of the multipoint flight conditions [50, 51]. In general, there is a substantial difference between optimized single point and multipoint results, even for a small multipoint stencil. Adding more flight conditions to the multipoint stencil typically produces diminishing returns in terms of the additional improvement in the optimized result for a standard non-morphing wing. Given the active adaptability of a morphing wing, the performance dependence on the stencil selection is less clear. Performing the 7-point optimization will help us better understand this relationship.

The multipoint stencils are detailed in Tables 1 and 2 below. The Mach number and lift coefficient ranges used in the stencil span a large portion of the typical flight regime. The altitude variations in the 7-point stencil are selected to correspond to full and empty aircraft weights. We select the stencils to produce a wide variety of flight conditions so that they can effectively demonstrate the benefits of the morphing trailing edge capability.

The nominal flight condition for the uCRM is at a Mach number of 0.85 and a lift coefficient (C_L) of 0.5. The multipoint stencils are centered around this nominal flight condition. We use the Breguet range equation to approximate the fuel burn:

$$\text{FB} = \text{LGW}\left(\exp\left(\frac{R\ \text{TSFC}}{V\frac{L}{D}}\right) - 1\right), \tag{1}$$

which is computed for each flight condition in the stencil. Here, LGW is the landing gross weight, R is the mission range, TSFC is the engine specific fuel consumption, V is the cruise speed, and L/D is the lift-to-drag ratio.

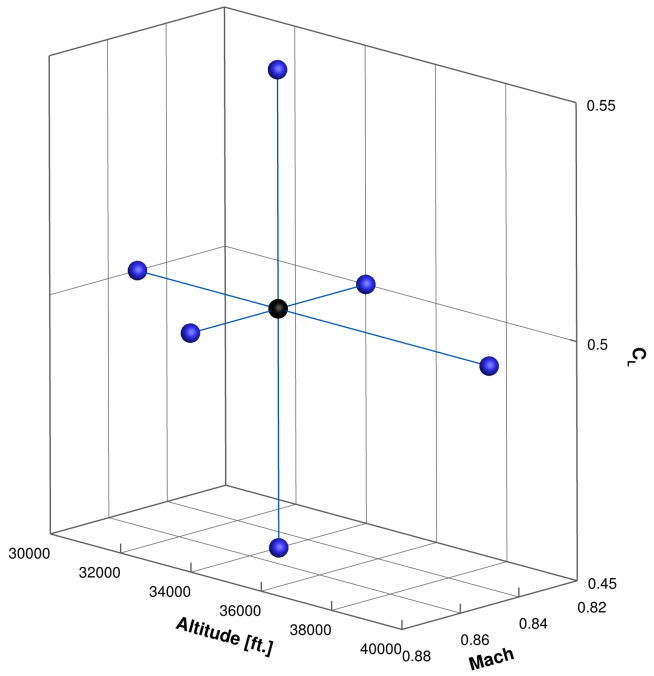

Figure 3: The 3-point stencil is a subset of the 7-point stencil shown here.

The objective of each of the optimizations is to minimize the average fuel burn over each of the cruise conditions in the multipoint stencil. To do this, the optimizer adjusts several design variables. These design variables are listed in Table 3. The angle of attack can be set at each flight condition (cruise and maneuver) so that each lift constraint is satisfied. The tail rotation angle is adjusted to trim the aircraft. The shape of the wing is controlled through adjustments of the FFD control points. There are 192 shape design variables that define the non-morphed, nominal optimized wing shape. These variables are available in each of the four optimizations. They adjust the z-location of control points only, preserving the planform of the aircraft. The FFD used for these optimizations is shown in Figure 1.

A subset of 64 shape variables defines the morphing device. As such, 64 variables are added for each non-nominal flight condition. For the 3-point stencil, this results in 256 additional shape variables: 64 for each of the two non-nominal

Flight condition	**Mach**	C_L	**Altitude (ft)**
Nominal	0.85	0.50	34,000
Low C_L	0.85	0.45	34,000
High C_L	0.85	0.55	34,000
Low M	0.82	0.50	34,000
High M	0.88	0.50	34,000
Low altitude	0.85	0.50	30,000
High altitude	0.85	0.50	40,000

Table 2: Overview of the 7-point stencil of cruise flight conditions. This stencil is shown in Mach–Altitude–C_L space in Figure 3.

cruise conditions and the two maneuver conditions. Wing twist variables are also defined (as aggregate movements of control points) at eight spanwise locations to give the optimizer more direct control of the twist distribution.

Shape changes are limited by a number of geometric constraints, which can also be found in Table 3. The volume of the wing is constrained not to decrease, ensuring sufficient space for fuel. At 20 spanwise locations, the leading edge and trailing edge thicknesses are constrained not to decrease, to provide low speed performance and manufacturability, respectively. Additional thickness constraints provide room for mounting actuation mechanisms to the aft spar and limit shape changes in the morphing region. Shear twist is avoided by constraining the movements of the leading and trailing edge control points.

Finally, 854 structural variables allow the optimizer to adjust thicknesses of spars, skins, ribs, and stiffeners. Maneuver conditions at 2.5 and $-1.0\,\mathrm{g}$ are considered to appropriately size the wingbox. The structure is constrained not to buckle at either maneuver condition and is constrained not to fail at the $2.5\,\mathrm{g}$ pull up condition. These constraints are aggregated using KS functions to limit the number of required adjoint solutions. Length variables are also provided to the structural model, but they are constrained to be consistent with the geometric lengths through a series of consistency constraints. Finally, 696 linear adjacency constraints ensure that thicknesses do not change by more than 5 mm between adjacent components of the structure.

	Function/variable	Description	3C	3M	7C	7M
minimize	Fuel burn					
w.r.t.	x_{α_c}	Cruise angle of attack	3	3	7	7
	x_{α_m}	Maneuver angle of attack	2	2	2	2
	x_{shape}	Wing shape (FFD)	192	192	192	192
	x_{morph}	Morphing shape (FFD)	0	256	0	512
	x_{twist}	Wing twist	8	8	8	8
	x_{tail}	Tail rotation angle	5	5	9	9
	x_{struct}	Structural sizing	854	854	854	854
		Total DVs	**1064**	**1320**	**1072**	**1584**
subject to	$L = n_i W$	Lift	5	5	9	9
	$M = 0$	Pitching moment	5	5	9	9
	$V/V_{\text{init}} \geq 1$	Fuel volume	1	1	1	1
	$t/t_{\text{init}}\|_{\text{LE}} \geq 1$	Leading edge thickness	20	20	20	20
	$t/t_{\text{init}}\|_{\text{TE}} \geq 1$	Trailing edge thickness	20	20	20	20
	$t/t_{\text{init}}\|_{\text{spar}} \geq 1$	Morphing thickness	20	220	20	220
	$\Delta z_{\text{LE}_u} = -\Delta z_{\text{LE}_l}$	Fixed leading edge	8	8	8	8
	$\Delta z_{\text{TE}_u} = -\Delta z_{\text{TE}_l}$	Fixed trailing edge	8	0	8	0
	$L_{\text{panel}} - x_{\text{panel}} = 0$	Panel consistency	272	272	272	272
	$\text{KS}_{\text{stress}} \leq 1$	Maneuver stress	3	3	3	3
	$\text{KS}_{\text{buckling}} \leq 1$	Maneuver buckling	6	6	6	6
	$\|x_{s_i} - x_{s_{i+1}}\| \leq 5\text{mm}$	Adjacency constraints	696	696	696	696
		Total constraints	**1064**	**1256**	**1072**	**1264**

Table 3: Overview of the 3-point conventional (**3C**), 3-point morphing (**3M**), 7-point conventional (**7C**), and 7-point morphing (**7M**) optimization problems.

4. Results

We now describe the results of these optimizations. We start by considering the results for the conventional and morphing 3-point optimizations. After that we consider the analogous results for the 7-point optimizations. Finally, we compare those results using a smaller morphing device and a configuration with a higher aspect ratio.

4.1. Three-point optimization

Figure 4 shows a comparison of the optimized conventional wing and the optimized wing with morphing for the 3-point stencil. The addition of morphing

had a clear positive effect on the performance of the wing, as the average fuel burn was reduced by 2.53%. This reduction is largely due to a substantial 22.4% reduction in structural weight. Looking at the pressure contours on the top of the wing for each of the cruise flight conditions, we see that in both optimizations there are few shocks, and the pressure distribution is consistent with optimal transonic results with a smooth pressure recovery [24].

The front view of the aircraft shows displaced wing shapes at the nominal cruise case as well as both maneuver conditions. We see that the addition of morphing at the maneuver conditions reduced the wing deflection at maneuver, which is consistent with the structural weight reduction we mentioned before. To see how this is achieved, we refer to the lift distribution below the front view of the aircraft. The distributions at the nominal cruise case and the 2.5 g maneuver overlay an elliptical lift distribution (in gray). The wing with morphing is able to shift more of the maneuver load inboard, reducing the root bending moment on the wing, which results in a much lighter structure.

Lower on Figure 4, we see the twist distributions, which show that the conventional wing washes out the tip using aeroelastic coupling at maneuver, while the wing with morphing produces a twist distribution more closely matching that at cruise. This is because adjustable camber handles the inboard shift of the load for the wing with morphing.

The thickness distribution of the structural members shows that the structure is thinner almost everywhere (where it is not limited by minimum gauge thickness) with the addition of morphing. The structural failure contours show that adding morphing allows the optimizer to push more structural members closer to their failure point, spreading the relatively localized stress and buckling concentrations seen in the conventional case. Finally, considering the slices labeled A–D, we see further confirmation of the results discussed before, along with the mechanism by which the morphing achieves these results. Again, there are results for the nominal case and the 2.5 g maneuver case. Considering the pressure distributions on the slices, we see typical results for most cases, except the maneuver condition with morphing. For this case, the pressure distributions

on the outboard section of the wing have inverted over the morphed region. To see the cause of this phenomenon, we analyze the airfoil shapes and pressure distributions. In the upper right corner of each plot is a zoomed-in view of the aft 20% of the airfoil. Here, we distinctly see the result of the morphing. At the maneuver condition, the morphing adds reverse camber on the outboard sections of the wing, producing the pressure distribution inversion and the inboard shift of the load distribution. This is the mechanism through which the wing with morphing reduces its structural weight, rather than relying solely on aeroelastic coupling like the conventional wing.

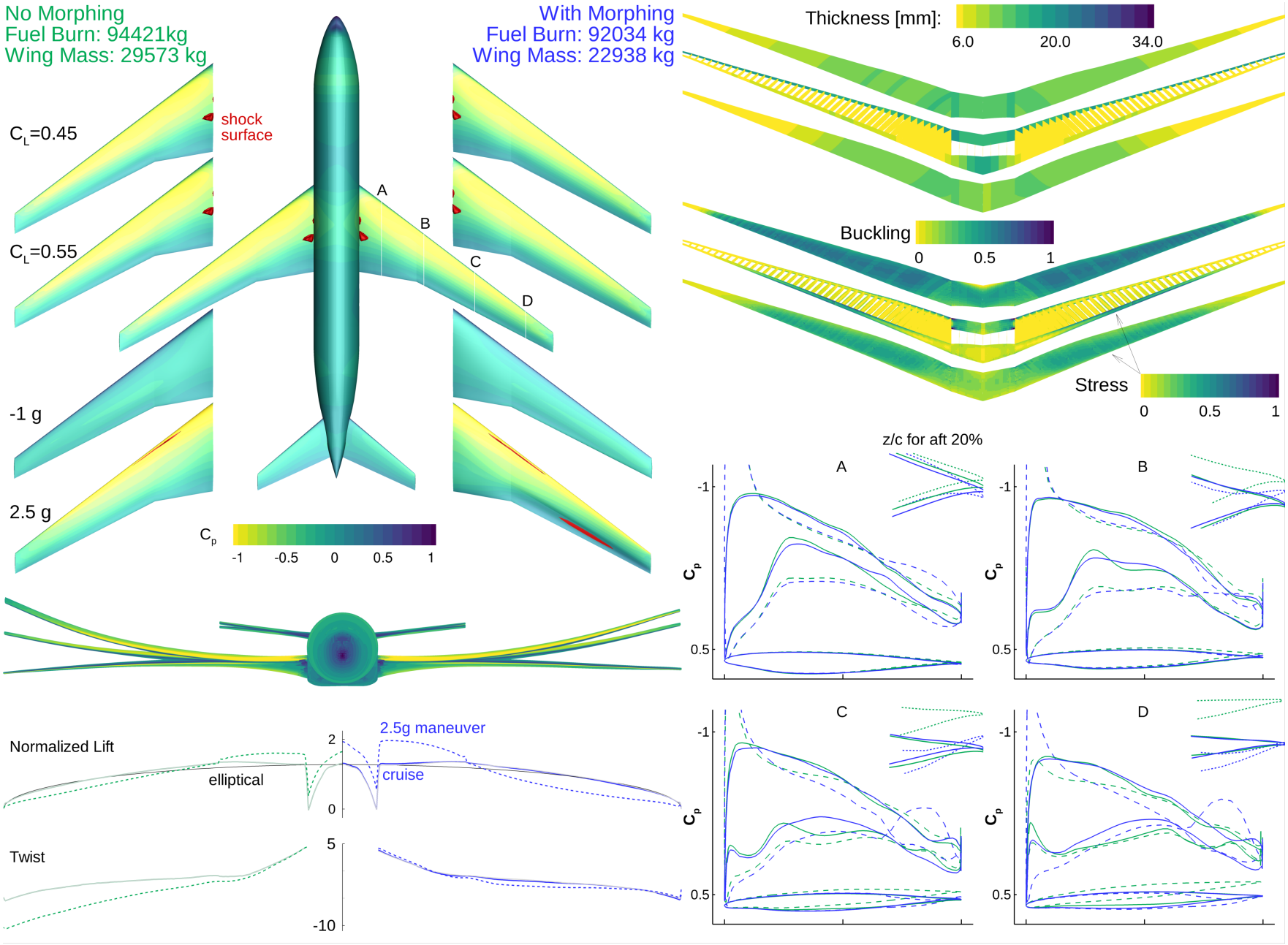

Figure 4: Adding morphing for the 3-point stencil reduced the fuel burn by 2.53% and the structural weight by 22.4%.

4.2. Seven-point optimization

The results in this section consist of the same optimization as before except for the 7-point stencil. Looking at the optimization results (Figure 5), we see many of the same trends as for the 3-point optimization. Again, the addition of morphing led to a substantial fuel burn reduction, this time by more than 5%, largely through the reduction of structural weight. As in the 3-point case, this reduction was enabled by the inboard shift of the maneuver load distribution resulting from the negative camber added to the outboard sections of the wing by the morphing. This mechanism for improving the aircraft performance seems to be the same in the two morphing cases; however, we can gather a few more insights by examining the results in more detail.

Looking at the structural weights of the two wings optimized with morphing, we see that the optimal 7-point wing has a lighter structure. This was unexpected because the maneuver conditions and structural constraints used in both cases were the same. That is, both structures were sized so that the wing would not buckle or fail in either the 2.5 g pull up or the -1.0 g push over maneuvers. This discrepancy suggests that in the 7-point case, there is an increased incentive to reduce the structural weight. To understand why, we consider the objective function: the average fuel burn of the cruise conditions as estimated by the Breguet range equation (1). According to that equation, there are two methods for reducing fuel burn: improving the aerodynamic performance at the cruise conditions (by increasing lift-to-drag ratio), and reducing the structural weight of the aircraft (which reduces the weight, LGW). These are the two mechanisms a morphing trailing edge can use to decrease the fuel burn and thus improve the objective function of the optimizations. These two mechanism do not work independently: Reductions in drag at cruise can lead to increased structural weight, which makes this trade-off difficult to handle without effective multidisciplinary design optimization.

We have already discussed the process by which morphing can reduce the structural weight. Morphing can also improve fuel burn through improvements to the aerodynamic performance at cruise. Without morphing, the wing shape is

forced to compromise to achieve good performance at all of the flight conditions; however, the inclusion of morphing reduces the coupling between aerodynamic performance at various flight conditions. This can be seen in the solid-lined pressure contours in Figure 5, which show the pressure distributions for the nominal flight condition with (blue) and without (green) morphing. For the conventional wing, the pressure contours show the waviness typical of multipoint optimizations, which are due to the compromise made between the various flight conditions. After morphing is added, the contours become much smoother. This illustrates the weakening of the coupling between flight conditions that is enabled by morphing.

The optimization of a wing with morphing for minimum fuel burn is a balance between improving aerodynamic performance at cruise and reducing structural weight. While morphing helps reduce the coupling between flight conditions, that coupling is not completely removed. The portion of the wing forward of the morphing is the same for all flight conditions, and the thicknesses of the wingbox members cannot change in flight. Within this context, the lower structural weight for the 7-point result provides an interesting insight. With the addition of cruise flight conditions, the balance between improving aerodynamic performance and reducing structural weight shifts towards the latter. Since there were no changes made to the constraints on the structure, this implies that the aerodynamic improvements available in the 7-point case are smaller than those available in the 3-point case. This conclusion makes sense, given the coupling between aerodynamic performance caused by the non-morphing section of the wing. Extrapolating this trend to consider aerodynamic performance of an aircraft over its full operational range, the weight reductions made possible by morphing become increasingly important. While morphing provides aerodynamic improvements through adaptability at a wide range of cruise conditions, its ability to substantially reduce structural weight through adaptive maneuver load alleviation yields a lighter structure that reduces fuel burn at all flight conditions.

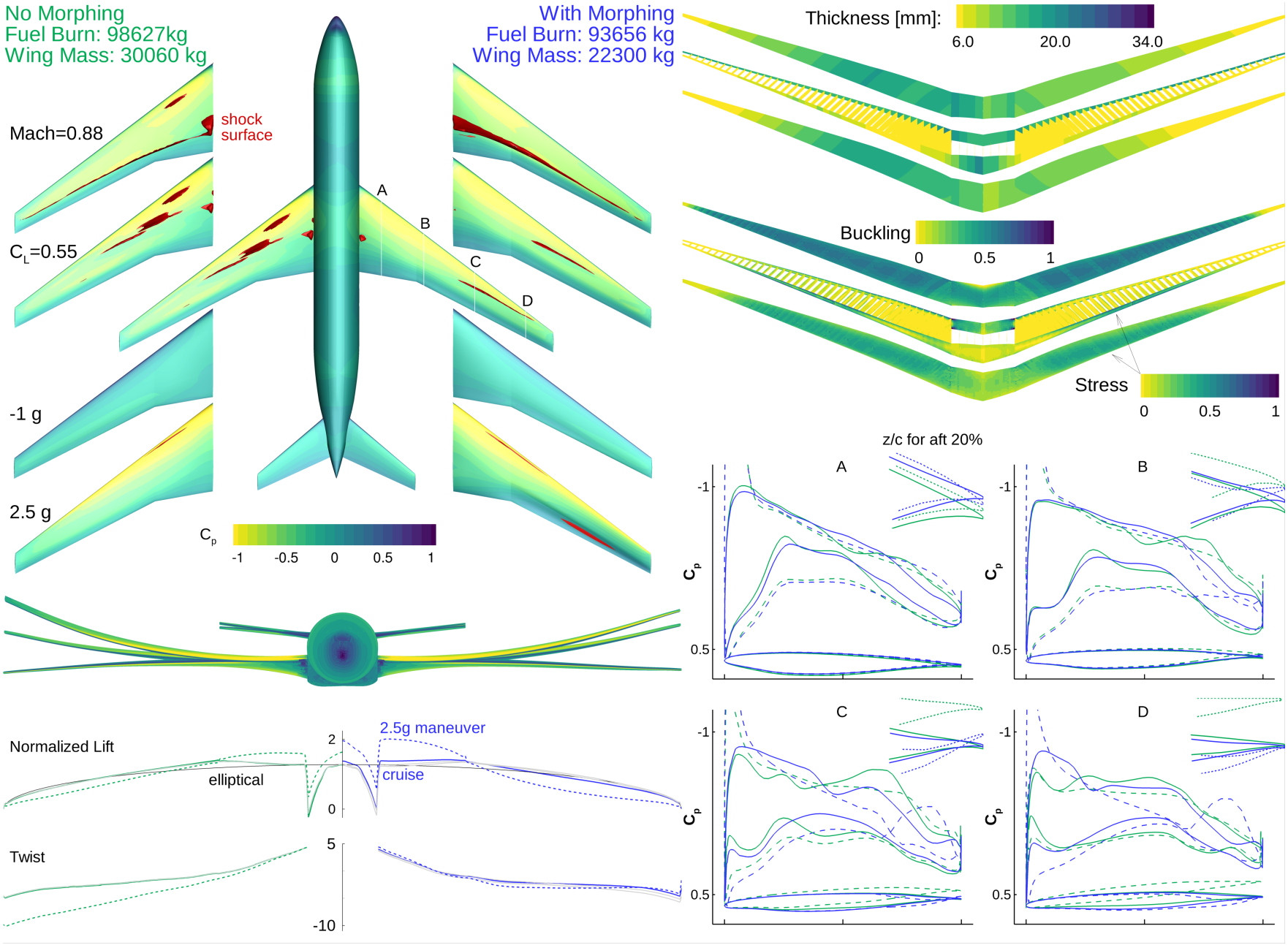

Figure 5: Adding morphing for the 7-point stencil reduced the fuel burn by 5.04% and the structural weight by 25.8%.

4.3. Effect of smaller morphing devices

In this subsection, we discuss two additional optimizations that resulted from reducing the size of the morphing device from the aft 40% of the chord to the aft 30%. The problem definition and setup for the 30% optimizations were similar to the previously discussed morphing optimization, except that the number of control points with active morphing freedom was reduced by half, thus limiting the size of the morphing device. We conducted these optimizations to gain some insight into the significance of the size of the morphing devices on the overall performance. Figures 6 and 7 show comparisons between the uCRM wing optimized with a 30% and 40% morphing trailing edge for the 3-point and 7-point stencils, respectively. The results for the 40% morphing device are the same as were shown in Figures 4 and 5.

The reduction of the morphing devices produced small increases in both the wing mass and the fuel burn. As would be expected with a smaller morphing device, the maneuver load alleviation was slightly less effective, resulting in a 2.78% heavier structure and 0.22% larger fuel burn compared to the wing with the larger morphing devices. The general result trends match those for the 40% morphing device, again showing a lower structural weight for the 7-point case due to the previously detailed balance between reducing structural weight and improving cruise performance. While there is a reduction in savings for a smaller morphing device, when compared to the wing without morphing, the improvements are still significant, showing that even if a morphing device is unable to extend all the way to the aft edge of the wingbox, it can still be an effective fuel burn reduction mechanism.

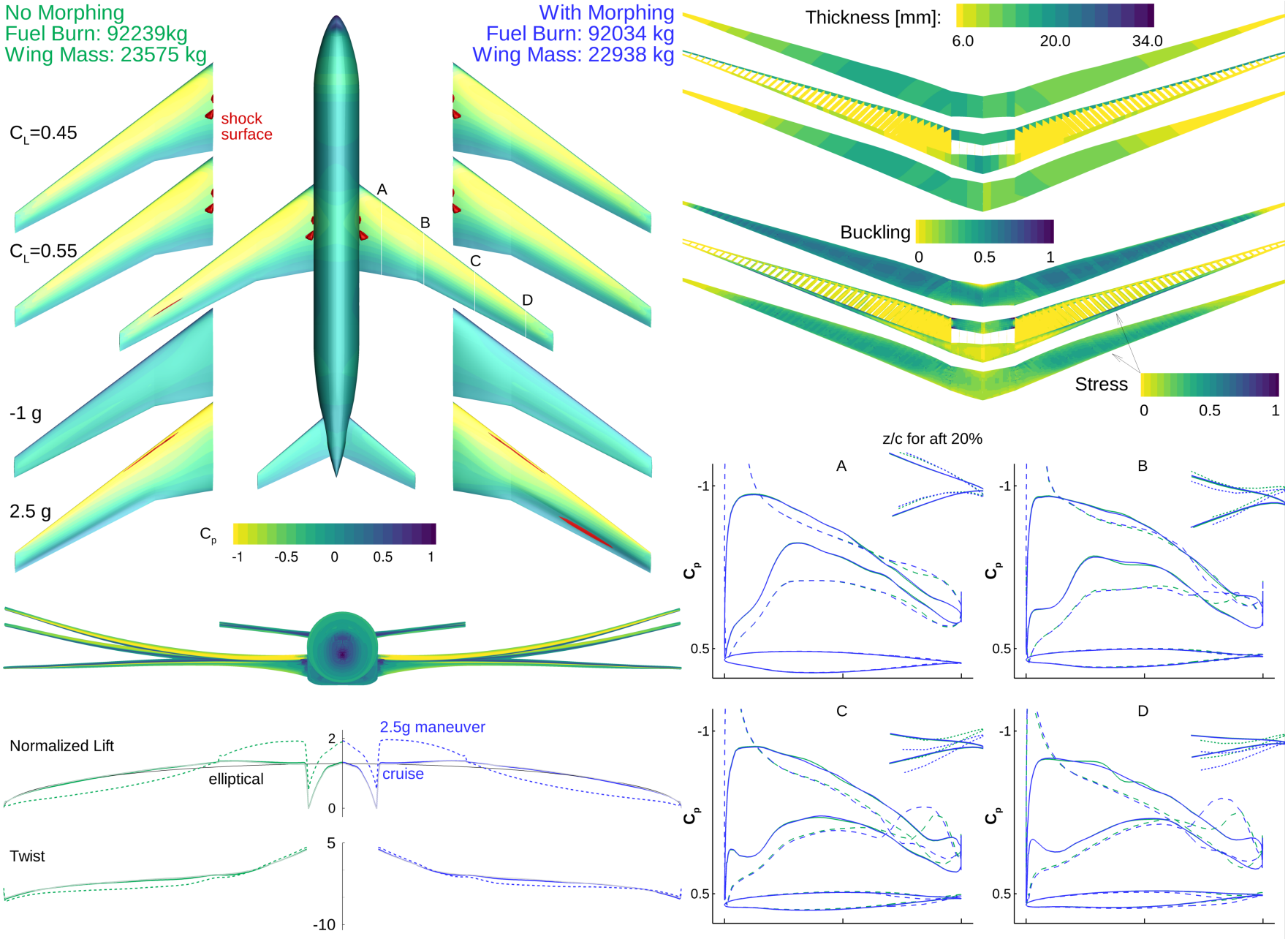

Figure 6: For the 3-point stencil when the morphing devices were reduced from 40% to 30% of the chord, the fuel burn increased by 0.22% and the wing mass increased by 2.78%.

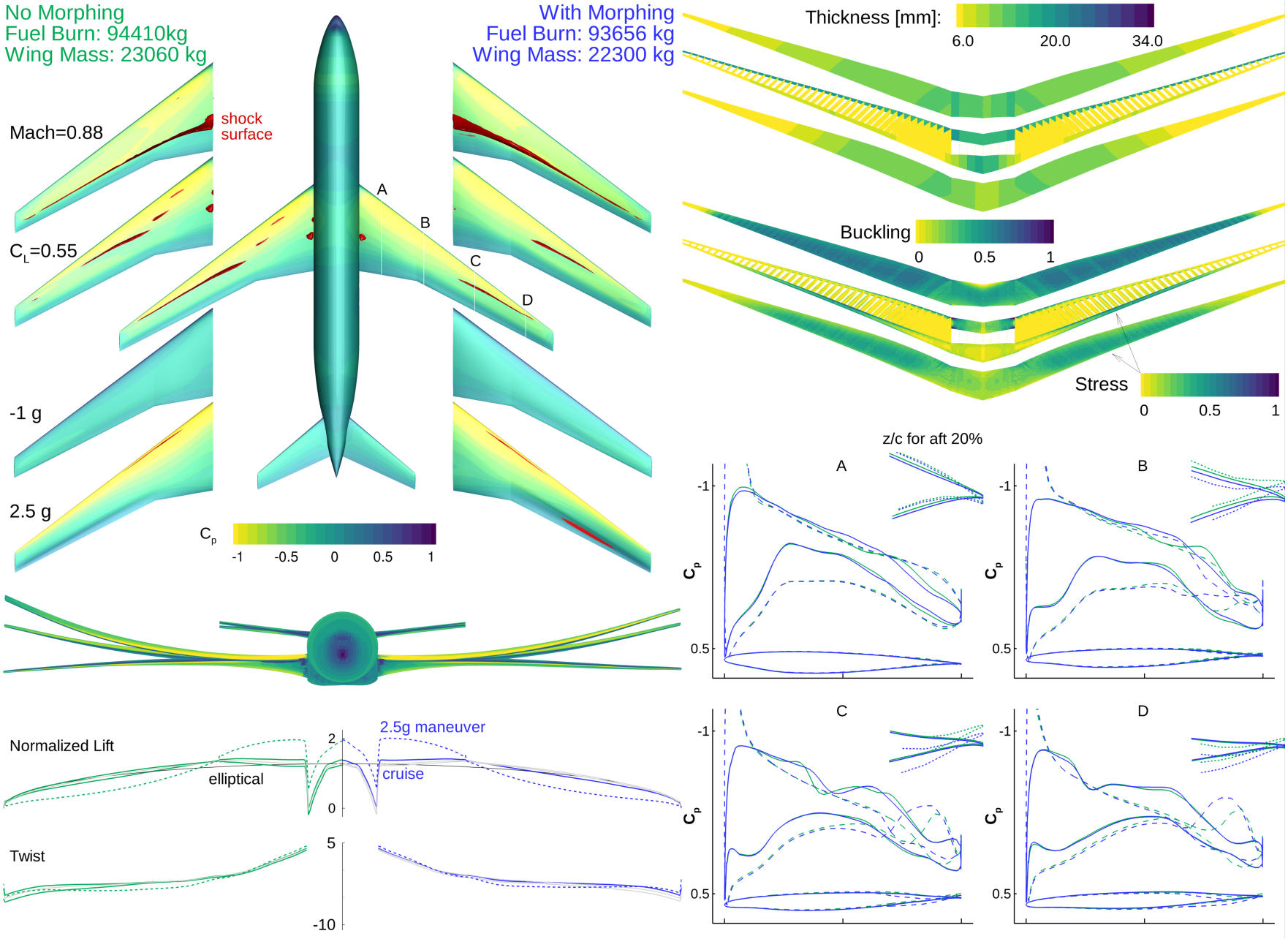

Figure 7: For the 7-point stencil when the morphing devices were reduced from 40% to 30% of the chord, the fuel burn increased by 0.81% and the wing mass increased by 3.41%.

4.4. Morphing optimization of a higher aspect ratio wing

Given the results of the morphing optimizations of the uCRM discussed above, it follows that the fuel burn savings provided by morphing trailing edge technology should increase as the flexibility of the wing increases. As material science and structural composite design continue to progress, the development of lighter and stronger next-generation aircraft structures is expected to enable higher aspect ratio wings. In aerostructural optimization, there is a trade-off between the aerodynamic induced drag benefit and the structural penalty from increasing wing span [32, 52]. Decreasing the weight or increasing the strength of structural components shifts the balance in this trade-off, increasing the optimal span. As such, we expect the current trend to continue and future aircraft wings to be more flexible and have higher aspect ratios. Thus, determining definitively the relationship between wing flexibility and the effectiveness of morphing technology is an important task. That is the objective of this section.

In this section, we discuss two design optimizations. The first optimization is a conventional wing optimized to provides a baseline design. The second optimization is the same as the baseline one with the addition of morphing design variables. The baseline configuration for these optimizations is the uCRM-13.5 [34], a configuration based on the uCRM that increases the aspect ratio from 9 to 13.5.

The morphing devices for this optimization again span the aft 40% of the wing. The FFD and control points used for these optimizations are shown in Figure 8.

To verify the hypothesis that increasing the aspect ratio of a wing increases the effectiveness of the adaptive morphing, we consider a 3-point optimization much like the one described in Table 3. The optimization results confirm the assumption that morphing trailing edge devices are more effective for higher aspect ratio wings. Comparing the results in Figure 9 to those from previous optimizations, we again see many of the same trends. The morphing produced substantial fuel burn reductions due largely to a shift of the maneuver load distribution inboard. Comparing the results in Figure 9 to those in Figure 4, we

see that the percentage reduction in structural weight is nearly identical (22.2% vs 22.4% for the high and low aspect ratio wings, respectively). However, the fuel burn reduction is more significant for the high aspect ratio case (3.79% versus 2.53%), so the morphing in the high aspect ratio optimization provides more substantial aerodynamic improvements. As the aspect ratio increases, the wing becomes more flexible, providing more opportunity for morphing devices to improve performance. The larger structural deformations in the high aspect ratio wing cause larger variations in the aerodynamic performance with respect to the flight conditions. This effect can be countered by the adaptive morphing device. It is clear that through maneuver load alleviation and increased aerodynamic robustness, morphing trailing edge technology can help enable higher aspect ratio wing design in future aircraft.

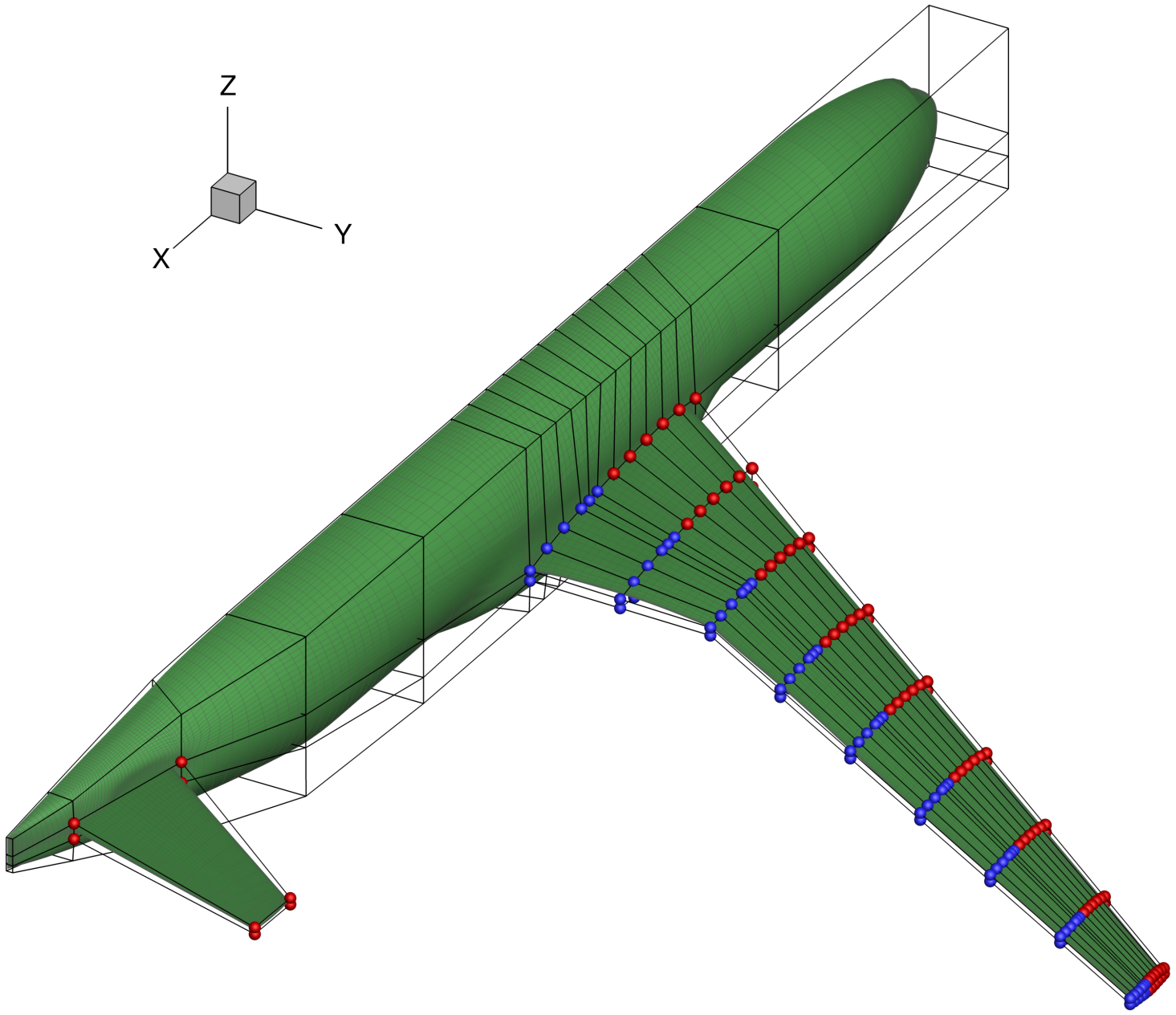

Figure 8: The FFD used for the uCRM-13.5 optimizations includes morphing variables (in blue) on the aft 40% of the wing.

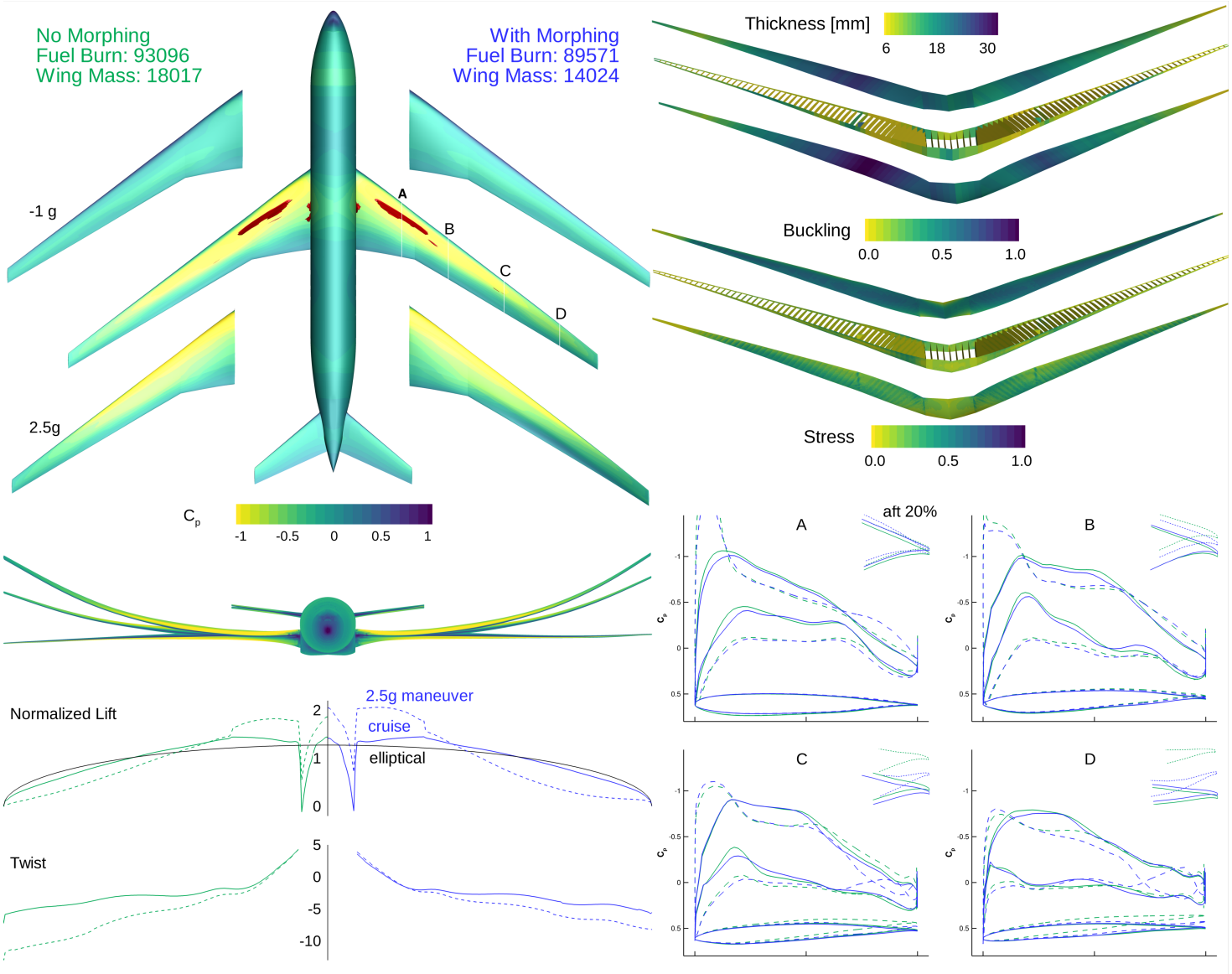

Figure 9: Adding a morphing trailing edge device to the high aspect ratio uCRM enabled a 22.2% reduction in structural weight and produced a fuel burn savings of 3.79%.

5. Summary

In this paper, we solve a number of multipoint aerostructural design optimizations that clearly demonstrate the value of morphing technology. These multipoint optimizations are summarized in Table 4.

Stencil	**Morphing**	**Fuel Burn** [kg]	**Wing Mass** [kg]
3 point	No	94,421	29,573
	Yes	92,034	22,938
7 point	No	98,627	30,060
	Yes	93,656	22,300

Table 4: As the multipoint stencil size is increased from 3 to 7 points, the fuel burn savings increases from 2.53% to 5.04%, respectively.

In our previous single point studies [28], the morphing design decreased fuel burn by 0.358% relative to the non-morphing baseline. The 3-point optimization in this study yielded much better results, as the addition of morphing reduced fuel burn by 2.53%. This comparison of the benefits of morphing technology on 1-point and 3-point (and 2 maneuver) optimizations clearly demonstrates that single point optimizations are insufficient to quantify the benefits enabled by morphing technology. While aeroelastic tailoring effectively designs an aircraft for a single cruise and a single maneuver condition, its ability to design a wing for additional conditions is limited. Bend-twist coupling can be used to tailor a wing for single point performance, but given the passive nature of this tailoring, the benefits become limited as additional flight conditions are considered. The addition of morphing adds the versatility the wing needs to perform more efficiently for a range of conditions, so a wing must be analyzed at multiple conditions to capture the benefits of morphing technology. When optimized for the 7-point stencil, the addition of morphing technology produced an even larger 5.04% fuel burn reduction.

The comparison between these optimizations also demonstrated the effect that morphing technology has on this wing weight trade-off. Without morphing, adding more points to the multipoint stencil produces a heavier and stiffer optimized wing, which helps maintain consistency in structural deformations at

the various cruise conditions, improving aerodynamic performance and thus fuel burn. This trend reverses with the addition of morphing: As more points are added to the multipoint stencil of a wing with morphing, the optimal structural weight is reduced. Because the morphing reduces the coupling between performance at various flight conditions, the benefit associated with increasing the consistency of the structural deformations is reduced. This can alternatively be considered as follows: Given that the morphing technology largely makes up for the aerodynamic cost of compromising for a multipoint stencil, the aerodynamic benefit associated with increasing the structural weight, and thus the consistency of the deformed wing shapes, is reduced. This in turn shifts the balance in the trade-off in wing structural weight, increasing the incentive to reduce the wing weight to save fuel burn.

Extrapolating this result further, since an aircraft does not need to perform well at a discrete set of flight conditions, but rather over the typical flight envelope, morphing technology clearly incentivizes a reduction in structural wing weight. At first glance, many understand that morphing technology increases the aerodynamic versatility of an aircraft and thus improves aerodynamic performance at a variety of flight conditions. These results demonstrate a more subtle conclusion: While there is an aerodynamic benefit due to the versatility of shape morphing, there is also a shift in the trade-off between weight and drag, incentivizing structural weight reductions. Given the maneuver load alleviation capabilities of morphing technology, this structural weight reduction becomes the major factor in the efficiency improvement provided by morphing for aircraft of this size.

Given the potential for restrictions on the size of the morphing devices, particularly in relation to the aft spar of the wing box, we included analogous morphing optimizations with a smaller morphing devices. These smaller devices spanned the aft 30% of the chord, leaving 10% of the chord between the morphing region and wing box for actuator mechanisms, high-lift devices, etc. While the smaller morphing mechanism was less effective, the increase in fuel burn with respect to the wing with the larger morphing mechanism was lim-

ited. For both the 3- and 7-point cases, the increase in fuel burn associated with the decrease in morphing device size was less than 1%, suggesting that the sensitivity of the performance with respect to morphing device size is small.

In our final multipoint optimization comparison, we sought to identify whether increasing the aspect ratio and flexibility of a wing would increase the effectiveness of morphing devices. A comparison of the fuel burn savings produced by adding a similar morphing trailing edge on a current-generation wing to those produced on a higher aspect ratio next-generation wing shows that morphing technology is clearly more effective for higher aspect ratio wings. This result is very important given the trend in aircraft design to move towards higher aspect ratio wings. There will be a synergistic effect developed by the use of next-generation structural materials and morphing trailing edge technology.

The optimization studies in this paper present a step towards accurately computing the potential for morphing technology to improve the fuel efficiency of transonic wings. The coupled optimization of high fidelity aerodynamic and structural models navigates the trade-offs between structural weight and aerodynamic robustness, and demonstrated clear benefit from reduced structural weight with the addition of an adaptive morphing trailing edge device. The benefits quoted herein are not associated with a specific morphing mechanism, but rather an idealistic morphing mechanism capable of any morphing shape within the FFD-defined design space with a weight comparable to that of conventional control actuators. This provides an upper bound on the benefits of morphing and informs future designs of morphing devices, but it does not provide the ability to include device weight in the optimization loop. More comprehensive future studies should include the weight of the morphing mechanism, which would likely shift the balance between aerodynamic performance and structural weight. Mechanism sizing would additionally require implementation of the associated constraints, like power requirements from mission and control system optimization, along with the necessary adjoint derivative calculations. Future studies may also consider the feasibility of the lighter structures optimized herein with respect to flight conditions that were not considered in this

study, like gust and flutter.

Acknowledgements

The authors would like to thank their collaborators at NASA, who supported this work through award NNX11AI19A. This work used the Extreme Science and Engineering Discovery Environment (XSEDE), which is supported by National Science Foundation grant number ACI-1053575 [53].

References

[1] Brooks, T. R., Kennedy, G. J., and Martins, J. R. R. A., "High-fidelity Multipoint Aerostructural Optimization of a High Aspect Ratio Tow-steered Composite Wing," *Proceedings of the 58th AIAA/ASCE/AHS/ASC Structures, Structural Dynamics, and Materials Conference, AIAA SciTech Forum*, Grapevine, TX, January 2017. doi:10.2514/6.2017-1350.

[2] Jutte, C. V., Stanford, B. K., Wieseman, C. D., and Moore, J. B., "Aeroelastic Tailoring of the NASA Common Research Model via Novel Material and Structural Configurations," *Proceedings of the AIAA 52nd Aerospace Sciences Meeting*, January 2014. doi:doi:10.2514/6.2014-0598.

[3] Carossa, G. M., Ricci, S., De Gaspari, A., Liauzun, C., Dumont, A., and Steinbuch, M., "Adaptive Trailing Edge: Specifications, Aerodynamics, and Exploitation," *Smart Intelligent Aircraft Structures (SARISTU)*, edited by P. C. Wölcken and M. Papadopoulos, Springer International Publishing, Cham, 2016, pp. 143–158.

[4] Kota, S., Hetrick, J., Osborn, R., Paul, D., Pendleton, E., Flick, P., and Tilmann, C., "Design and Application of Compliant Mechanisms for Morphing Aircraft Structures," *Proceedings of the SPIE Smart Structures and Materials Conference*, San Diego, CA, March 2003.

[5] Hetrick, J. A., Osborn, R. F., Kota, S., Flick, P. M., and Paul, D. B., "Flight Testing of Mission Adaptive Compliant Wing," *Proceedings of the 48th AIAA/ASME/ASCE/AHS/ASC Structures, Structural Dynamics, and Materials Conference*, Honolulu, HI, April 2007, AIAA 2007-1709.

[6] Kota, S., Osborn, R., Ervin, G., Maric, D., Flick, P., and Paul, D., "Mission Adaptive Compliant Wing–Design, Fabrication and Flight Test," *RTO Applied Vehicle Technology Panel (AVT) Symposium*, 2009.

[7] Kota, S., Flick, P., and Collier, F. S., "Flight Testing of FlexFloil Adaptive

Compliant Trailing Edge," *54th AIAA Aerospace Sciences Meeting, AIAA SciTech Forum*, San Diego, CA, January 2016. doi:10.2514/6.2016-0036.

[8] Lebofsky, S., Ting, E., and Nguyen, N., "Aeroelastic Modeling and Drag Optimization of Aircraft Wing with Variable Camber Continuous Trailing Edge Flap," *Proceedings of the 32nd AIAA Applied Aerodynamics Conference*, Atlanta, GA, June 2014.

[9] Kaul, U. K. and Nguyen, N. T., "Drag Optimization Study of Variable Camber Continuous Trailing Edge Flap (VCCTEF) Using OVERFLOW," *32nd AIAA Applied Aerodynamics Conference, AIAA Aviation Forum*, No. AIAA 2014–2444, 2014.

[10] Bowman, J., Sanders, B., and Cannon, B., "Development of Next Generation Morphing Aircraft Structures," *48th Proceedings of the AIAA/ASME/ASCE/AHS/ASC Structures, Structural Dynamics, and Materials Conference*, Honolulu, HI, April 2007.

[11] Sofla, A. Y. N., Meguid, S. A., Tan, K. T., and Yeo, W. K., "Shape Morphing of Aircraft Wing: Status and Challenges," *Materials & Design*, Vol. 31, No. 3, 3 2010, pp. 1284–1292. doi:10.1016/j.matdes.2009.09.011.

[12] Barbarino, S., Bilgen, O., Ajaj, R. M., Friswell, M. I., and Inman, D. J., "A Review of Morphing Aircraft," *Journal of Intelligent Material Systems and Structures*, Vol. 22, 2011, pp. 823–877. doi:10.1177/1045389X11414084.

[13] Friswell, M. I., "Hierarchical Models of Morphing Aircraft," *Proceedings of the 23rd International Conference on Adaptive Structures and Technologies*, Nanjing, China, October 2012.

[14] Greff, E., "The development and design integration of a variable camber wing for long/medium range aircraft," *Aeronautical Journal*, November 1990, pp. 301–312.

[15] Pendleton, E. W., Bessette, D., Field, P. B., Miller, G. D., and Griffin, K. E., "Active Aeroelastic Wing Flight Research Program: Technical Pro-

gram and Model Analytical Development," *Journal of Aircraft*, Vol. 37, No. 4, 2000, pp. 554–561.

[16] Weisshaar, T. A., "Morphing Aircraft Systems: Historical Perspectives and Future Challenges," *Journal of Aircraft*, Vol. 50, No. 2, 2013, pp. 337–353. doi:10.2514/1.C031456.

[17] Yang, J., Sartor, P., Cooper, J. E., and Nangia, R. K., "Morphing Wing Design for Fixed Wing Aircraft," *56th AIAA/ASCE/AHS/ASC Structures, Structural Dynamics, and Materials Conference*, American Institute of Aeronautics and Astronautics, January 2015. doi:10.2514/6.2015-0441.

[18] Martins, J. R. R. A., *Encyclopedia of Aerospace Engineering*, Vol. Green Aviation, chap. Fuel burn reduction through wing morphing, Wiley, October 2016, pp. 75–79. doi:10.1002/9780470686652.eae1007.

[19] Hanselka, H., "A Lightweight Concept for Aerodynamic Surfaces With Variable Camber," *21st ICAS Congress*, No. A98-31620, Melbourne, Australia, September 1998.

[20] Monner, H., Sachau, D., and Breitbach, E., *Design aspects of the elastic trailing edge for an adaptive wing*, Defense Technical Information Center, 2000.

[21] Molinari, G., Quack, M., Dmitriev, V., Morari, M., Jenny, P., and Ermanni, P., "Aero-Structural Optimization of Morphing Airfoils for Adaptive Wings," *Journal of Intelligent Material Systems and Structures*, Vol. 22, No. 10, 2011, pp. 1075–1089. doi:10.1177/1045389X11414089.

[22] Molinari, G., Quack, M., Arrieta, A. F., Morari, M., and Ermanni, P., "Design, realization and structural testing of a compliant adaptable wing," *Smart Materials and Structures*, Vol. 24, 2015, pp. 105027. doi:10.1088/0964-1726/24/10/105027.

[23] Lyu, Z., Kenway, G. K. W., and Martins, J. R. R. A., "Aerodynamic Shape Optimization Investigations of the Common Research Model Wing

Benchmark," *AIAA Journal*, Vol. 53, No. 4, April 2015, pp. 968–985. doi:10.2514/1.J053318.

[24] Lyu, Z. and Martins, J. R. R. A., "Aerodynamic Shape Optimization of an Adaptive Morphing Trailing Edge Wing," *Journal of Aircraft*, Vol. 52, No. 6, November 2015, pp. 1951–1970. doi:10.2514/1.C033116.

[25] Wakayama, S. and White, E. V., "Evaluation of Adaptive Compliant Trailing Edge Technology," *33rd AIAA Applied Aerodynamics Conference*, Dallas, TX, June 2015. doi:10.2514/6.2015-3289.

[26] Stanford, B. K., "Static and Dynamic Aeroelastic Tailoring with Variable-Camber Control," *Journal of Guidance, Control, and Dynamics*, Vol. 39, No. 11, 2016, pp. 2522–2534. doi:10.2514/1.G000413.

[27] Martins, J. R. R. A. and Lambe, A. B., "Multidisciplinary Design Optimization: A Survey of Architectures," *AIAA Journal*, Vol. 51, No. 9, September 2013, pp. 2049–2075. doi:10.2514/1.J051895.

[28] Burdette, D., Kenway, G. K. W., Lyu, Z., and Martins, J. R. R. A., "Aerostructural Design Optimization of an Adaptive Morphing Trailing Edge Wing," *Proceedings of the AIAA Science and Technology Forum and Exposition (SciTech)*, Kissimmee, FL, January 2015. doi:10.2514/6.2016-1294.

[29] Kenway, G. K. W., Kennedy, G. J., and Martins, J. R. R. A., "Scalable Parallel Approach for High-Fidelity Steady-State Aeroelastic Analysis and Derivative Computations," *AIAA Journal*, Vol. 52, No. 5, May 2014, pp. 935–951. doi:10.2514/1.J052255.

[30] Chen, S., Lyu, Z., Kenway, G. K. W., and Martins, J. R. R. A., "Aerodynamic Shape Optimization of the Common Research Model Wing-Body-Tail Configuration," *Journal of Aircraft*, Vol. 53, No. 1, January 2016, pp. 276–293. doi:10.2514/1.C033328.

[31] Gray, J., Mader, C. A., Kenway, G. K. W., and Martins, J. R. R. A., "Modeling Boundary Layer Ingestion Using a Coupled Aeropropulsive Analysis," *Journal of Aircraft*, Vol. 55, No. 3, 2018, pp. 1191–1199. doi:10.2514/1.C034601.

[32] Kenway, G. K. W. and Martins, J. R. R. A., "Multipoint High-Fidelity Aerostructural Optimization of a Transport Aircraft Configuration," *Journal of Aircraft*, Vol. 51, No. 1, January 2014, pp. 144–160. doi:10.2514/1.C032150.

[33] Liem, R. P., Kenway, G. K. W., and Martins, J. R. R. A., "Multimission Aircraft Fuel Burn Minimization via Multipoint Aerostructural Optimization," *AIAA Journal*, Vol. 53, No. 1, January 2015, pp. 104–122. doi:10.2514/1.J052940.

[34] Brooks, T. R., Kenway, G. K. W., and Martins, J. R. R. A., "Benchmark Aerostructural Models for the Study of Transonic Aircraft Wings," *AIAA Journal*, 2018. doi:10.2514/1.J056603, (In press).

[35] Dhert, T., Ashuri, T., and Martins, J. R. R. A., "Aerodynamic Shape Optimization of Wind Turbine Blades Using a Reynolds-Averaged Navier–Stokes Model and an Adjoint Method," *Wind Energy*, Vol. 20, No. 5, May 2017, pp. 909–926. doi:10.1002/we.2070.

[36] Garg, N., Kenway, G. K. W., Martins, J. R. R. A., and Young, Y. L., "High-fidelity Multipoint Hydrostructural Optimization of a 3-D Hydrofoil," *Journal of Fluids and Structures*, Vol. 71, May 2017, pp. 15–39. doi:10.1016/j.jfluidstructs.2017.02.001.

[37] Kenway, G. K., Kennedy, G. J., and Martins, J. R. R. A., "A CAD-Free Approach to High-Fidelity Aerostructural Optimization," *Proceedings of the 13th AIAA/ISSMO Multidisciplinary Analysis Optimization Conference*, No. AIAA 2010-9231, Fort Worth, TX, Sept. 2010. doi:10.2514/6.2010-9231.

[38] Sederberg, T. W. and Parry, S. R., "Free-form Deformation of Solid Geometric Models," *SIGGRAPH Comput. Graph.*, Vol. 20, No. 4, Aug. 1986, pp. 151–160. doi:10.1145/15886.15903.

[39] Uyttersprot, L., *Inverse Distance Weighting Mesh Deformation*, Ph.D. thesis, Delft University of Technology, 2014.

[40] van der Weide, E., Kalitzin, G., Schluter, J., and Alonso, J. J., "Unsteady Turbomachinery Computations Using Massively Parallel Platforms," *Proceedings of the 44th AIAA Aerospace Sciences Meeting and Exhibit*, Reno, NV, 2006, AIAA 2006-0421.

[41] Lyu, Z., Kenway, G. K., Paige, C., and Martins, J. R. R. A., "Automatic Differentiation Adjoint of the Reynolds-Averaged Navier–Stokes Equations with a Turbulence Model," *21st AIAA Computational Fluid Dynamics Conference*, San Diego, CA, Jul. 2013. doi:10.2514/6.2013-2581.

[42] Kennedy, G. J. and Martins, J. R. R. A., "A Parallel Finite-Element Framework for Large-Scale Gradient-Based Design Optimization of High-Performance Structures," *Finite Elements in Analysis and Design*, Vol. 87, September 2014, pp. 56–73. doi:10.1016/j.finel.2014.04.011.

[43] Lambe, A. B., Martins, J. R. R. A., and Kennedy, G. J., "An Evaluation of Constraint Aggregation Strategies for Wing Box Mass Minimization," *Structural and Multidisciplinary Optimization*, Vol. 55, No. 1, January 2017, pp. 257–277. doi:10.1007/s00158-016-1495-1.

[44] Kennedy, G. J. and Hicken, J. E., "Improved constraint-aggregation methods," *Computer Methods in Applied Mechanics and Engineering*, Vol. 289, No. 0, 2015, pp. 332 – 354. doi:10.1016/j.cma.2015.02.017.

[45] Brown, S. A., "Displacement Extrapolation for CFD+CSM Aeroelastic Analysis," *Proceedings of the 35th AIAA Aerospace Sciences Meeting*, Reno, NV, 1997, AIAA 1997-1090.

[46] Martins, J. R. R. A., Alonso, J. J., and Reuther, J. J., "A Coupled-Adjoint Sensitivity Analysis Method for High-Fidelity Aero-Structural Design," *Optimization and Engineering*, Vol. 6, No. 1, March 2005, pp. 33–62. doi:10.1023/B:OPTE.0000048536.47956.62.

[47] Gill, P. E., Murray, W., and Saunders, M. A., "SNOPT: An SQP algorithm for large-scale constrained optimization," *SIAM Journal of Optimization*, Vol. 12, No. 4, 2002, pp. 979–1006. doi:10.1137/S1052623499350013.

[48] Perez, R. E., Jansen, P. W., and Martins, J. R. R. A., "pyOpt: A Python-Based Object-Oriented Framework for Nonlinear Constrained Optimization," *Structural and Multidisciplinary Optimization*, Vol. 45, No. 1, January 2012, pp. 101–118. doi:10.1007/s00158-011-0666-3.

[49] Yu, Y., Lyu, Z., Xu, Z., and Martins, J. R. R. A., "On the Influence of Optimization Algorithm and Starting Design on Wing Aerodynamic Shape Optimization," *Aerospace Science and Technology*, Vol. 75, April 2018, pp. 183–199. doi:10.1016/j.ast.2018.01.016.

[50] Liem, R. P., Martins, J. R. R. A., and Kenway, G. K., "Expected Drag Minimization for Aerodynamic Design Optimization Based on Aircraft Operational Data," *Aerospace Science and Technology*, Vol. 63, April 2017, pp. 344–362. doi:10.1016/j.ast.2017.01.006.

[51] Kenway, G. K. W. and Martins, J. R. R. A., "Multipoint Aerodynamic Shape Optimization Investigations of the Common Research Model Wing," *AIAA Journal*, Vol. 54, No. 1, January 2016, pp. 113–128. doi:10.2514/1.J054154.

[52] Kennedy, G. J. and Martins, J. R. R. A., "A parallel aerostructural optimization framework for aircraft design studies," *Structural and Multidisciplinary Optimization*, Vol. 50, No. 6, December 2014, pp. 1079–1101. doi:10.1007/s00158-014-1108-9.

[53] Towns, J., Cockerill, T., Dahan, M., Foster, I., Gaither, K., Grimshaw, A., Hazlewood, V., Lathrop, S., Lifka, D., Peterson, G. D., Roskies, R., Scott, J. R., and Wilkins-Diehr, N., "XSEDE: Accelerating Scientific Discovery," *Computing in Science & Engineering*, Vol. 16, No. 5, September 2014, pp. 62–74. doi:10.1109/MCSE.2014.80.